

Brewing Stronger Features: Dual-Teacher Distillation for Multispectral Earth Observation

Filip Wolf Blaž Rolih Luka Čehovin Zajc
University of Ljubljana, Faculty of Computer and Information Science, Slovenia
filip.wolf@fri.uni-lj.si

Abstract

Foundation models are transforming Earth Observation (EO), yet the diversity of EO sensors and modalities makes a single universal model unrealistic. Multiple specialized EO foundation models (EOFMs) will likely coexist, making efficient knowledge transfer across modalities essential. Most existing EO pretraining relies on masked image modeling, which emphasizes local reconstruction but provides limited control over global semantic structure. To address this, we propose a dual-teacher contrastive distillation framework for multispectral imagery that aligns the student’s pretraining objective with the contrastive self-distillation paradigm of modern optical vision foundation models (VFMs). Our approach combines a multispectral teacher with an optical VFM teacher, enabling coherent cross-modal representation learning. Experiments across diverse optical and multispectral benchmarks show that our model adapts to multispectral data without compromising performance on optical-only inputs, achieving state-of-the-art results in both settings, with an average improvement of 3.64 percentage points in semantic segmentation, 1.2 in change detection, and 1.31 in classification tasks. This demonstrates that contrastive distillation provides a principled and efficient approach to scalable representation learning across heterogeneous EO data sources. Code: [TBA](#).

1. Introduction

Foundation models (FMs) have recently emerged as a powerful paradigm in Earth Observation (EO), demonstrating strong transferability across diverse downstream tasks [1, 20, 56]. They leverage large volumes of unlabeled data [53, 56, 65], reduce reliance on scarce or inconsistent labels [10, 18, 29, 50], and enable flexible task adaptation [8, 44, 59]. These qualities are particularly valuable in EO, where data collection is abundant but high-quality annotations are limited [34].

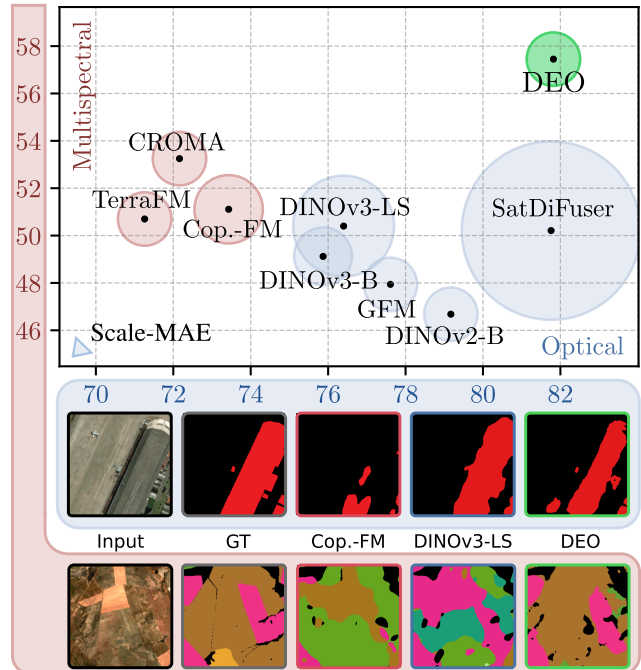


Figure 1. DEO, our proposed dual-teacher pretraining approach, results in a model that achieves state-of-the-art results in **multi-spectral** EO tasks while maintaining performance on **optical** EO tasks. On top, we demonstrate our performance in optical and multispectral semantic segmentation, visualizing model size using colored circles. Below, the first row of images shows qualitative results for the optical SpaceNetv1 [52] dataset, while the second row shows results for the multispectral m-SA-crop-type dataset [33].

However, developing a single, universal EO foundation model (EOFM) remains challenging [63]. EO data vary widely in spatial resolution, spectral characteristics, and acquisition conditions, while geographic and seasonal variations further introduce domain shifts [3, 10, 43, 59, 63], rendering the training of a single model that effectively captures the intricacies of various EO data difficult. Instead, progress increasingly depends on *efficient knowledge trans-*

fer between models [7], and knowledge distillation provides a practical mechanism for achieving this.

EOFMs for multispectral (MS) satellite imagery are a strong target for improvement by distillation. They contain the optical (RGB) channels that can be well-represented by modern general-purpose vision foundation models (VFMs) [49, 53], which are prime candidates for knowledge extraction. On the other hand, EOFMs can also additionally encode rich spectral information from MS data, which is required for many EO applications. Since training a new EOFM from scratch on MS data is computationally expensive [40, 49], leveraging existing VFMs becomes an appealing alternative. However, knowledge transfer must be done correctly to maximize its effectiveness.

In the broader computer vision community, modern large VFMs are typically trained using contrastive and self-distillation objectives [11, 40, 49] that explicitly shape global semantics and produce latent feature spaces well-suited for downstream transfer. In contrast, much of EO pretraining still relies on masked image modeling (MIM) [16, 37, 56], which emphasizes local reconstruction [27, 61] and imposes weaker constraints on global semantic structure. Consequently, contrastive and self-distillation approaches remain comparatively underexplored in EO [1, 53, 65]. Motivated by the observation, we propose a **contrastive dual-teacher** distillation framework for MS representation learning. Our method pairs (i) a contrastive self-distillation multispectral teacher that structures the MS feature space and (ii) an optical VFM teacher that provides high-level semantic priors learned at a global scale. Because the student and the optical teacher share compatible pretraining objectives, the student’s latent space more readily matches that of the VFM compared to pairing distillation with an MIM objective. This compatibility yields more coherent cross-modal transfer and better downstream performance. Our contributions are as follows:

- We introduce a *dual-teacher pretraining strategy* that unifies a contrastive self-distillation multispectral teacher with distillation from an optical teacher, combining global representation learning with transfer of semantic priors.
- We demonstrate that matching the student’s pretraining objective with that of a VFM teacher (e.g., DINOv3) enables a more effective and data-efficient transfer of optical priors to a multispectral student.

Our model, **DEO** (*Distillation for Earth Observation*), achieves state-of-the-art performance across optical and multispectral downstream tasks, with an average improvement of 3.64 percentage points in semantic segmentation, 1.2 points in change detection, and 1.31 points in classification. This highlights distillation-centric training as a key strategy for building a sustainable and interoperable landscape of EO foundation models.

2. Related Work

Contrastive learning and distillation. Contrastive Learning (CL) is a widely used technique for self-supervised learning responsible for many breakthroughs in the field [6, 11, 13, 24, 26, 64]. In contrast to MIM-based methods such as Masked Autoencoders (MAE) [5, 27, 61], CL leads to strong semantic representations invariant to distribution shifts. While sensitive to the choice of data augmentation and prone to dimensional collapse, recent advances have aimed to mitigate these drawbacks [58].

As large pretrained foundation models rose in prominence, so did the concept of distillation. It is primarily used to transfer knowledge between models, with usage being divided into compressing large pretrained models into smaller ones [28, 39, 40, 42, 47, 49, 58] or improving newer models [25, 28, 37, 42, 56]. Recently, the closely-related representation learning technique of self-distillation was used to train advanced VFMs [11, 40, 49, 66].

Vision Foundation Models. General-purpose VFMs have demonstrated strong performance across many downstream tasks with minimal fine-tuning, even without task-specific training [23, 37, 53, 55]. This is largely due to a key commonality between these models: extensive pretraining on large image corpora and careful data curation [32, 40, 41, 49]. Recent large VFMs, such as DINOv2 [40] and DINOv3 [49], were trained on more than 100 million curated images and have demonstrated a capacity to consistently improve results in various domains [4, 57], with DINOv3 showing a strong focus on the EO domain. The development of VFMs pushes boundaries not only in terms of methodology but also in protocols for input data collection and preparation. Effectively utilizing the strong general representations present in VFMs is a great asset for many specialized domains, including EO.

Earth Observation Foundation Models. Most EOFM proposed in recent years were pretrained using MIM-based techniques [2, 16, 35, 37, 43, 56, 62] and an ever-increasing amount of unlabeled EO data. Less common approaches explore alternative representation learning techniques, such as CL [1, 18, 20, 21, 50, 53], JEPa [3], and diffusion [29, 30]. Pioneering methods such as Scale-MAE [43], while notable for establishing the field, were limited to optical data and simple MAE-style pretraining. CROMA [21] was among the first to utilize CL to achieve strong results by combining modalities, while recently, TerraFM [1] and SatDiFuser [29] utilized modern representation learning techniques on diverse input data to achieve strong results.

Due to the perceived domain shift, VFM distillation has only recently been explored in EO [25, 37]. The recently proposed Copernicus-FM [56] combines MIM-style pretraining with DINOv2-based distillation. However, its

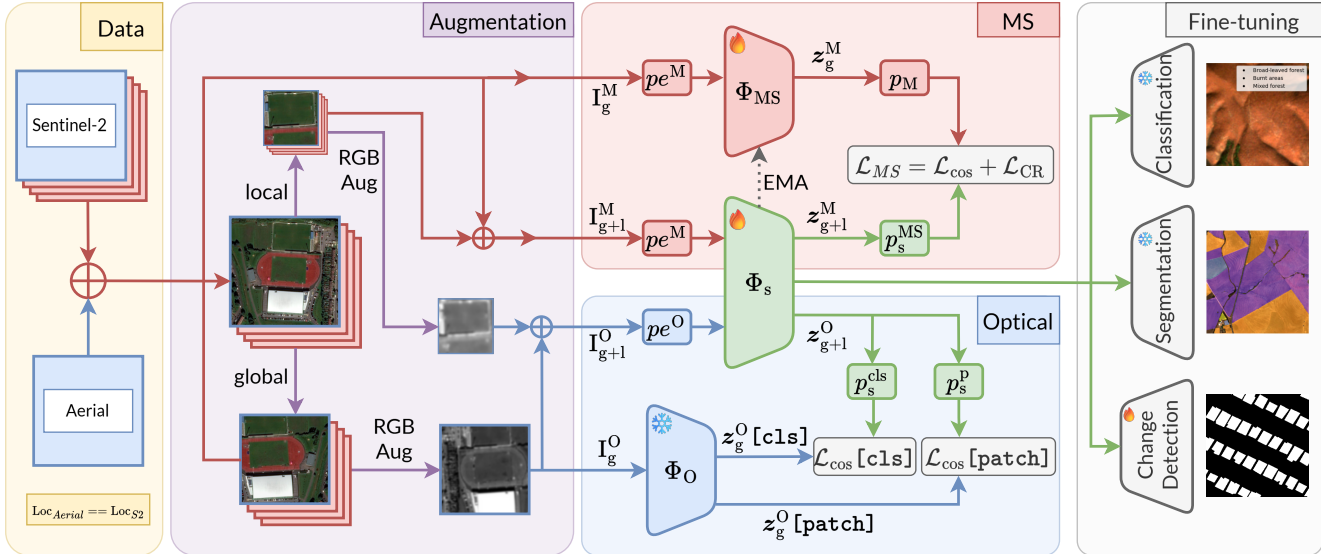


Figure 2. **Overview of the double-distillation pretraining approach.** The pretraining dataset utilizes a standard FMoW Sentinel-2 dataset, augmented with high-resolution aerial images where possible. Random crops and other augmentation operations are performed on sampled images. Full multispectral and optical channel subsets are used for their corresponding distillation branches. The multispectral branch is a contrastive learning setup where the teacher is updated using EMA. In the optical branch, distillation is done using a frozen VFM teacher. The resulting model can then be used in various downstream tasks.

reconstruction-driven objective is not fully aligned with the contrastive and distillation losses used to train modern VFMs [40, 49], resulting in a weaker global semantic structure of features. In contrast, we integrate VFM distillation into a contrastive pretraining pipeline, ensuring objective-level consistency with the teacher.

3. Methodology

We propose a pretraining approach that excels at diverse downstream tasks when multispectral data is available, without compromising performance on tasks that use only the optical bands (i.e., RGB) of an image. As shown in Figure 2, our approach uses a contrastive self-distillation student-teacher framework with *two* teachers. One teacher specializes in teaching students optical representations, while the other specializes in teaching students robust multispectral representations. Together, they train a single student network to excel in both input modalities. To aid in clarity, we use different colored notation for different parts of the network: a **red** color for the **multispectral** teacher, **blue** for the **optical** teacher, and **green** for the **student**. In the following sections, we provide an introduction to contrastive self-distillation and describe each component of the network.

3.1. Contrastive self-distillation

The core part of our method (red section in Figure 2) is based on DINO [11], a self-supervised pretraining method

designed for learning global data representations. DINO is a *contrastive* method: it works by aligning the representations generated from different *views* (i.e., various crops) of the same input image and ensuring their similarity. It is also *self-distilling*, as the teacher’s weights are an *exponential moving average* (EMA) of the student’s weights, which are updated in turn using backpropagation. This mechanism provides effective representation learning, while also preventing the teacher’s and student’s weights from diverging [14, 24, 26, 58].

We enforce similarity between representations of different image views using a *compression loss* such as cosine similarity. This, however, can lead to *representation collapse* on its own, where both the teacher and student predict constant vectors (e.g., zero vectors) [24], since no constraint is put on the structure of the embedding space. To prevent this from happening we additionally use an *expansion loss* in the form of a *coding rate regularizer* [58]. The main idea is to maintain diversity in the representation space by penalizing a low-rank covariance matrix of the features, forcing the model to spread information across all feature dimensions instead of collapsing to trivial vectors. Concretely, we do this by forcing the log-determinant of the diagonal between the covariance matrix of the network features and the unit vector to be as large as possible, i.e., by minimizing $\mathcal{L}_{CR} := -\log \det(\mathbf{I} + \text{Cov}[\mathbf{z}])$.

3.2. Crafting diverse inputs

We generate diverse augmented views of input images (purple section in Figure 2) to learn a stronger feature space [13, 64]. We use multi-channel Sentinel-2 imagery I^M as input, where the first three channels represent the optical (RGB) part of an image, i.e. $I^O \subset I^M$. For each I^M , the following augmentation pipeline is applied. We first lightly augment I^M with channel-agnostic augmentations like flipping, denoted as A_M . We then additionally augment I^O with heavy augmentations A_O , such as color jitter, Gaussian blur, and solarization, to ensure robustness to input perturbations.

From this augmented image, we create n larger *global* views I_g^M and m smaller *local* views I_l^M using cropping and resizing. To teach MS representations, we concatenate I_g^M and I_l^M into I_{gUl}^M for the student, while the MS teacher obtains only the global views I_g^M . For teaching optical representations, we use the optical images I_{gUl}^O for the student, while the teacher again receives only the global part I_g^O . Formally:

$$I_{gUl}^M = I_g^M \cup I_l^M, I_{gUl}^O = I_g^O \cup I_l^O, I_{gUl}^O \subset I_{gUl}^M, \quad (1)$$

where

$$\begin{aligned} I_g^M &= g(A_M(I^M)), I_l^M = l(A_M(I^M)), \\ I_g^O &= g(A_O(I^O \subset A_M(I^M))), \\ I_l^O &= l(A_O(I^O \subset A_M(I^M))). \end{aligned} \quad (2)$$

Here, g is the function used for creating global views, and l is for local views. All augmentations are performed randomly for each input image.

3.3. Learning multispectral representations

We utilize the method described in Section 3.1 to learn strong multispectral representations, shown in red in Figure 2. We start by passing I_g^M to the multispectral teacher encoder Φ_{MS} and I_{gUl}^M to the student encoder Φ_s (notice that Φ_s receives both local and global image views), employing a 10-channel patch embedding layer before the encoders. Φ_{MS} and Φ_s produce features $\Phi_{MS}(I_g^M) = z_g^M$ and $\Phi_s(I_{gUl}^M) = z_{gUl}^M$, which are then projected into a common feature space via projection heads p_M for Φ_{MS} and p_s^{MS} for Φ_s . Adding small projection heads improves performance and training stability compared to computing loss directly on backbone outputs [11]. We can then formulate the loss function for learning MS features, as

$$\begin{aligned} \mathcal{L}_{MS} &= \mathcal{L}_{\cos}(p_M(z_g^M), p_s^{MS}(z_{gUl}^M)) \\ &\quad - \gamma \mathcal{L}_{CR}(p_M(z_g^M), p_s^{MS}(z_{gUl}^M)), \end{aligned} \quad (3)$$

where \mathcal{L}_{\cos} represents *cosine similarity*, \mathcal{L}_{CR} is the *coding rate regularizer* described in Section 3.1, and γ is a weighting coefficient.

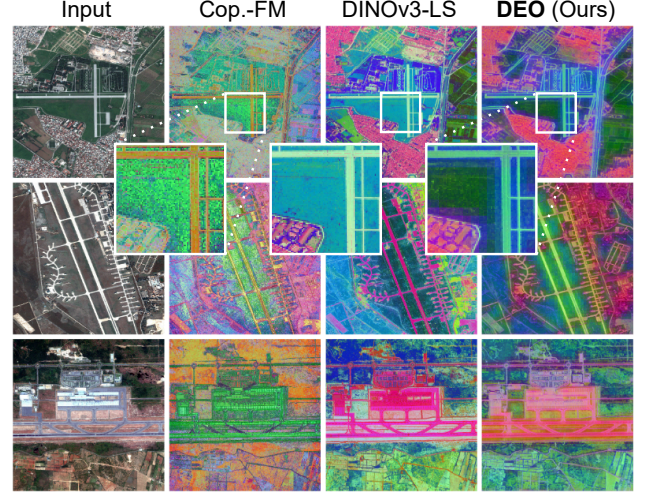


Figure 3. **PCA feature visualization and comparison** between Copernicus-FM [56], DINOv3-LS [49], and DEO (ours). We note the similarity of our method’s features to those of DINOv3.

3.4. Incorporating optical knowledge

The objective described in Section 3.3 is well-suited for learning MS representations, but falls short in producing the fine-grained, pixel-level features required for dense prediction tasks such as segmentation and change detection. Additionally, without dedicated optical supervision, the model does not develop specialized optical representations comparable to those learned by large optical VFMs [49, 53]. To bridge this gap, we introduce a VFM as a second teacher, enabling the student to unify multispectral and optical knowledge within a single representation space. Unlike prior works that combine masked image modeling (MIM) with VFM distillation [37, 56], our objective from Equation (3) is inherently compatible with the training paradigm of modern VFMs such as DINOv3, which also rely on contrastive self-distillation. As illustrated by the feature PCA visualization in Figure 3, the student’s latent space aligns more closely to that of DINOv3 compared to the MIM-based Copernicus-FM, leading to more compatible feature transfer and improved downstream performance.

We introduce VFM distillation by expanding on the network described in Section 3.3. We pass I_g^O to the optical VFM teacher Φ_O and I_{gUl}^O to the student Φ_s , mirroring our MS learning part of the network whilst using a separate 3-channel patch embedding layer for optical data before the encoder. To incorporate both global and pixel-level knowledge from Φ_O , we distill the class token $[cls]_F$ and patch tokens $[p]_F$ from its final layer, as well as patch tokens $[p]_{mid}$ from an intermediate layer into corresponding student features. To achieve this, we introduce distinct projection heads p_s^{cls} , p_s^{p1} , and p_s^{p2} for the student, which are separate from those used during MS training. This both aligns

Method	Optical					Multispectral					Overall Avg
	SN	GB-cattle	GB-pv	GB-chesa.	Avg	GB-SA-c.	GB-cas.	S1F11	PASTIS	Avg	
DINOv2-B [40] _{RGB}	79.76	76.75	94.30	65.86	79.17	29.39	54.51	87.92	14.89	46.68	62.92
DINOv3-B [49] _{RGB}	79.06	73.01	94.34	64.04	77.61	30.82	57.87	87.50	15.58	47.94	62.78
DINOv3-LS [49] _{RGB}	78.67	72.86	94.04	60.03	76.40	33.05	63.32	88.78	16.45	50.40	63.40
Scale-MAE [43] _{RGB}	76.24	51.66	91.45	33.33	63.17	23.13	59.42	84.77	6.70	43.50	53.33
GFM [37] _{RGB}	77.30	62.12	93.56	70.49	75.87	29.79	62.59	85.42	18.66	49.12	62.49
SatDiFuser [29] _{RGB}	77.17	82.98	95.30	71.60	81.76	32.60	66.50	84.08	17.65	50.21	65.99
CROMA [21] _{MS}	71.82	74.37	88.00	54.43	72.16	34.27	59.91	94.16	24.66	53.25	62.70
TerraFM [1] _{MS}	73.15	65.81	91.59	54.47	71.26	30.95	59.49	92.72	19.65	50.70	60.98
Cop.-FM [56] _{MS}	75.45	68.88	93.56	55.81	73.43	34.67	55.71	92.58	21.49	51.11	62.27
DEO (Ours)	80.83	80.21	94.41	72.47	81.98	37.96	68.56	94.32	28.96	57.45	69.72

Table 1. **Results on optical and multispectral segmentation datasets.** Methods take as input either 3-channel optical (RGB) bands or multi-channel MS bands. The GB prefix indicates that the dataset is from the GEO-Bench [33] benchmark, SN represents SpaceNetv1 [52], S1F11 is Sen1Floods11 [9], and PASTIS is from [22]. DINOv3-LS is the ViT-L version of DINOv3 pretrained on satellite imagery. All results are expressed in macro mIoU. First and second place results are marked. Further dataset details can be found in the Supplementary.

the feature dimension of the student to that of the teacher’s, while also decoupling the projection heads between the optical and MS learning tasks, which has been shown to improve performance [40]. We can then formulate the distillation loss for learning optical features as:

$$\begin{aligned}
\mathcal{L}_O = & \alpha_1 \mathcal{L}_{\cos}((z_g^O[\text{cls}]_F), p_s^{\text{cls}}(z_{gUI}^O[\text{cls}]_F)) \\
& + \alpha_2 \mathcal{L}_{\cos}((z_g^O[\text{p}]_F), p_s^{\text{p1}}(z_{gUI}^O[\text{p}]_F)) \\
& + \alpha_3 \mathcal{L}_{\cos}((z_g^O[\text{p}]_{\text{mid}}), p_s^{\text{p2}}(z_{gUI}^O[\text{p}]_{\text{mid}})),
\end{aligned} \quad (4)$$

and we obtain the final learning loss by minimizing both the MS and optical learning objectives:

$$\mathcal{L} = -\mathcal{L}_{MS} - \mathcal{L}_O. \quad (5)$$

We thereby train both multispectral and optical features in unison without compromising either feature space.

3.5. Implementation details

To aid in learning fine-grained features, we utilize the Swin [36] transformer as our backbone, leveraging its hierarchical architecture and input patch size of 4. Most VFMs utilize ViT [19] with a patch size of 16 as the standard backbone, which limits their feature resolution. However, we demonstrate that distilling a ViT-based VFM into a Swin-based backbone yields fine-grained features that combine the knowledge of an optical teacher and a dedicated MS teacher.

For creating *global* views of the input image, we crop in the range of $\{0.4, 1\}$ before resizing to an image size of 224×224 . For *local* views, we crop in the range of $\{0.05, 0.4\}$, and resize to 96×96 . Following [11], we set $n = 2$ and $m = 10$. We set $\alpha_1 = 1$, $\alpha_2 = 0.5$, $\alpha_3 = 0.5$, and $\gamma = 1$. Further training details are provided in the Supplementary.

3.6. Pretraining

We pretrain our method for 100 epochs using the Adam optimizer [31] and cosine learning rate scheduling on 16 NVIDIA A100 GPUs, with a batch size of 8 per GPU and a combined dataset of 500,000 images from the fMoW-Sentinel [16] and fMoW-RGB [15] datasets. To construct the dataset, we first remove the three 60m resolution atmospheric bands from Sentinel-2 imagery in fMoW-Sentinel, leaving 10 bands for pretraining. We then replace 150,000 low spatial resolution optical bands in Sentinel-2 imagery with their high spatial resolution aerial counterparts from fMoW-RGB at the same location, leading to improved performance on high spatial resolution datasets.

4. Results

We evaluate DEO on a diverse set of optical and multispectral segmentation, change detection, and classification datasets against state-of-the-art methods. To more clearly differentiate methods, we specify whether they take as input multi-channel MS data or only 3-channel optical (RGB). Further evaluation details can be found in the Supplementary.

4.1. Segmentation

To evaluate DEO’s ability to employ fine-grained features, we report semantic segmentation results in Table 1 using UPerNet [60] as a segmentation head on a frozen backbone [29, 50, 56]. Methods are evaluated on the benchmark suite GEO-Bench [33], along with additional datasets SpaceNetv1 [52], Sen1Floods11 [9], and PASTIS [22], creating a diverse mix of optical and MS datasets encompassing building, crop, flood, and animal segmentation. DEO achieves the best results in both modalities, with particularly remarkable average improvements of 4.20 points over

Method	Optical	MS	Avg
	LEVIR	OSCD	
DINOv2-B [40] _{RGB}	91.1	49.0	70.1
DINOv3-B [49] _{RGB}	91.6	55.2	73.4
DINOv3-LS [49] _{RGB}	91.7	57.2	74.5
Scale-MAE [43] _{RGB}	92.1	47.2	69.6
GFM [37] _{RGB}	89.8	54.1	72.0
SatDiFuser [29] _{RGB}	90.2	55.2	72.7
CROMA [21] _{MS}	88.5	52.3	70.4
TerraFM [1] _{MS}	89.5	57.5	73.5
Cop.-FM [56] _{MS}	90.7	58.7	74.7
DEO (Ours)	91.3	60.4	75.9

Table 2. **Results on optical and multispectral bi-temporal change detection datasets.** Methods take as input either 3-channel optical (RGB) bands or multi-channel MS bands. All results are expressed in binary F1 score considering only the change class. **First** and **second** place results are marked.

the state-of-the-art on MS datasets, thanks to our representation learning approach. This increase in MS performance is especially noticeable on tasks that benefit the most from MS data, such as crop and flood segmentation (GB-SA-c., PASTIS, and S1F11).

4.2. Change detection

We evaluate performance on remote sensing change detection using two well-established datasets, the optical LEVIR [12], and a multispectral OSCD [17] dataset. We follow the protocol from related work [37, 45, 54] and extract backbone features from a pair of pre- and post-event images, then fuse them using element-wise subtraction. Fused features are processed using a UPerNet [60] decoder to produce the final binary change map. We report the results in Table 2 using the binary F1 metric considering change class only [37, 45, 54]. DEO achieves the best performance in the MS setting, outperforming the previous best by 1.7 points, setting a new state-of-the-art. It also achieves competitive performance on optical settings. While methods like Scale-MAE [43] outperform it on optical data, DEO manages to balance MS and optical performance more effectively, overall achieving the best results.

4.3. Classification

To perform image classification, we extract class tokens or pooled patch tokens from the last layer of a frozen backbone and train a linear classifier on top of it. We report results on three diverse MS land cover datasets in Table 3. Our model achieves the overall best results, with an average performance 1.3 points above that of the next best-performing method. It also surpasses or closely matches the performance of the best-performing methods on individual

Method	Multispectral			
	GB-ben	GB-s2s	GB-es	Avg
DINOv2-B [40] _{RGB}	50.56	41.38	89.6	60.51
DINOv3-B [49] _{RGB}	55.48	52.94	93.3	67.91
DINOv3-LS [49] _{RGB}	58.70	48.68	92.4	66.59
Scale-MAE [43] _{RGB}	46.06	44.02	92.4	60.83
GFM [37] _{RGB}	51.91	47.26	95.5	64.89
SatDiFuser [29] _{RGB}	49.97	35.19	88.2	57.12
CROMA [21] _{MS}	53.13	46.65	89.3	63.69
TerraFM [1] _{MS}	62.15	47.57	93.1	67.61
Cop.-FM [56] _{MS}	45.65	44.93	87.9	59.49
DEO (Ours)	58.43	52.23	97.0	69.22

Table 3. **Results on multispectral classification datasets with linear probing.** Methods take as input either 3-channel optical (RGB) bands or multi-channel MS bands. The GB prefix indicates that the dataset is from the GEO-Bench [33] benchmark. GB-ben (m-bigearthnet) results are expressed in the F1 metric, while GB-s2s (m-so2sat) and GB-es (m-eurosat) results are expressed in Top-1 accuracy. **First** and **second** place results are marked.

Method	Average Rank			Param. size (M)	Pretrain Size (M)
	Optical	MS	Overall		
Scale-MAE [43]	8.0	8.3	8.2	303	0.36
GFM [37]	4.5	5.7	5.1	87	0.6
TerraFM [1]	6.5	3.5	5.0	85	18
DINOv2-B [40]	3.0	7.1	5.0	85	142
Cop.-FM [56]	5.8	4.0	4.9	139	18
CROMA [21]	6.7	3.0	4.8	85	1
DINOv3-B [49]	3.4	6.0	4.7	85	1689
DINOv3-LS [49]	3.8	5.5	4.6	303	493
SatDiFuser [29]	2.0	4.7	3.3	949	0.72
DEO (ours)	1.3	1.2	1.3	87	0.5

Table 4. **Summary of methods and results.** Ranks for all tested methods over benchmark datasets, averaged over optical datasets, multispectral (MS) datasets, and overall. **First** and **second** place results are marked. Additionally, model size and pretraining corpus size are provided for reference.

datasets.

4.4. Overall

In Table 4, we present the average rank for each tested method across all tasks on optical and MS datasets, as well as the overall average rank. DEO shows a strong overall lead, with a pronounced advantage in MS performance. The second-best performing method on optical tasks, SatDiFuser [29], significantly lags behind DEO in performance on MS tasks, despite having a model size more than 10 times larger. Two other methods we tested utilize distillation: Copernicus-FM [56] and GFM [37], with GFM also employing a Swin transformer. Due to our pretraining approach, described in Section 3, our method indirectly in-

Component	Optical		Multispectral		Overall	
	Avg	Improv.	Avg	Improv.	Avg	Improv.
Base (MS)	77.87		60.44		69.16	
+ DINOv3 [cls]	79.07	↑ 1.20	62.81	↑ 2.37	70.94	↑ 1.79
+ Sep. Opt. path	81.20	↑ 2.13	62.69	↓ 0.12	71.95	↑ 1.00
+ DINOv3 [p]	81.74	↑ 0.53	62.46	↓ 0.23	72.10	↑ 0.15
+ Optical Aug.	81.95	↑ 0.22	63.02	↑ 0.55	72.48	↑ 0.39
+ High Res. Optical	82.22	↑ 0.27	63.51	↑ 0.50	72.87	↑ 0.38

Table 5. Ablation study of DEO components on three optical and three multispectral datasets. We present average results for each dataset category, as well as overall averages. We also show relative improvement for each component. Best results are marked in **bold**.

corporates large amounts of data from VFMs in a manner that more carefully aligns feature spaces, resulting in a substantial performance lead over both methods, while using much less pretraining data. Remarkably, we outperform all tested versions of DINOv2 [40] and DINOv3 [49], including the ViT-Large-based version pretrained on satellite data, demonstrating our method’s ability to effectively incorporate optical VFM features with contrastive MS pretraining.

4.5. Ablation study

Component ablation. We introduce multiple components to our pretraining architecture to simultaneously learn **MS** and **optical** features without compromising either feature space. To better understand the impact of each component, we begin with a simple *contrastive self-distillation baseline* designed for learning MS features presented in Section 3.3 (Base (MS) in Table 5), and gradually build up to our state-of-the-art model. For consistency, each model is pretrained with a Swin-Tiny backbone on 50,000 images for 50 epochs and then fine-tuned on three optical (SN, GB-cattle, GB-pv) and three MS (GB-SA-c., GB-cas., S1F11) segmentation datasets. For each modality and overall, we present the average results, as well as the relative improvements over the previous iteration, in Table 5.

- **DINOv3 distillation.** We begin by naively distilling the DINOv3 [cls] [49] token into the student features in addition to the contrastive multispectral objective. This results in a substantial increase in performance for both modalities, as we distill knowledge from a large VFM, despite aligning the MS feature space to resemble the optical representations derived from the VFM.
- **Separate optical path.** Introducing an additional projection head p_s^{cls} and processing optical images in a separate pass with the student leads to a substantial improvement on optical tasks, while minimally degrading results for MS tasks. We attribute this to the optically derived DINOv3 features $z_g^{\text{O}}[\text{cls}]_F$ now being distilled into optically derived student features $z_{gU}^{\text{O}}[\text{cls}]_F$.

VFM	Optical	MS	Overall
DINOv2 [40]	85.01	62.71	73.86
DINOv3 [49]	85.03	62.77	73.90
RADIOv2.5 [28]	83.57	63.12	73.34

Table 6. Comparison of distillation backbones. Best results for each dataset category and overall are presented in **bold**.

- **Patch token distillation.** To increase alignment with DINOv3 further, we additionally distill DINOv3 [patch] tokens from the last and intermediate layers into last and intermediate stage student patch tokens $p_s^{p1}(z_{gU}^{\text{O}}[\text{p}]_F)$ and $p_s^{p2}(z_{gU}^{\text{O}}[\text{p}]_{\text{mid}})$, leading to an improvement in optical performance and slight degradation in MS performance. While distilling the class token from DINOv3 incorporates general knowledge, distilling patch tokens helps our model mimic the out-of-the-box linearly separable patch features present in DINOv3 [49].
- **Additional optical augmentations.** Introducing heavy augmentations A_O for the optical input images (Section 3.2) leads to an overall improvement. While CL methods generally benefit from strong augmentations, this also helps incorporate *robust* features from DINOv3, i.e., features that are less susceptible to input perturbations.
- **High-resolution optical data.** Replacing the low-resolution Sentinel-2 optical data with high-resolution aerial imagery leads to an overall increase in performance. This is especially noticeable on MS datasets, likely due to the high-resolution optical data being transferred to the lower-resolution MS data, thereby serving as privileged knowledge. It also provides more detailed features, which are usually useful for dense tasks that require high resolution.

Our additions to the baseline training pipeline significantly increase performance by an average of 4.35 points on optical and 3.07 points on MS tasks.

VFM distillation. Results for various VFM optical teachers used for distillation are shown in Table 6, averaged over four optical and four MS datasets. Besides DINOv3 [49], we evaluate DINOv2 [40] and RADIOv2.5 [28] which integrates features of multiple VFMs. DINOv2 and DINOv3 yield comparable results, although at large scales, distilling DINOv3 generally yields better performance. RADIOv2.5 performs slightly worse on optical datasets and better on

Method	10%		
	GB-SA-c.	GB-BEN	SpaceNetv1
DINOv2-B [40] _{RGB}	23.04	44.43	75.57
DINOv3-B [49] _{RGB}	25.22	46.52	74.36
DINOv3-LS [49] _{RGB}	27.83	47.84	74.75
Scale-MAE [43] _{RGB}	24.73	28.78	72.80
GFM [37] _{RGB}	22.82	33.99	72.57
SatDiFuser [29] _{RGB}	20.87	43.75	73.00
TerraFM [1] _{MS}	26.29	48.53	69.24
CROMA [21] _{MS}	26.81	40.72	68.27
Cop.-FM [56] _{MS}	28.15	28.71	71.65
DEO (Ours)	28.98	51.89	76.46

Table 7. **Results in a low-data regime (10%)**. Methods take as input either 3-channel optical (RGB) bands or multi-channel MS bands. The GB prefix indicates that the dataset is from the GEO-Bench [33] benchmark. GB-SA-c. and SpaceNetv1 [52] results are expressed in macro mIoU, while GB-BEN results are expressed in F1. First and second place results are marked.

MS datasets, but since the primary strength of VFMs lies in the optical domain, we opt to distill DINOv3 in our final model.

Low-data regime. We evaluate DEO under limited labeled data availability across three datasets. The results in Table 7 demonstrate that our method maintains strong performance even with limited fine-tuning, validating our choice to utilize contrastive learning, as it generally requires less fine-tuning to perform well compared to other pretraining paradigms [5, 48]. This is especially practical for tasks where collecting labels is challenging, e.g., when rapid response is required during natural disasters. [38, 51].

4.6. Qualitative results

Qualitative results for segmentation and change detection are shown in Figure 4. On SpaceNetv1 [52] and Sen1Floods11 [9], DEO captures fine detail that competing methods fail to capture, while on GB-SA-c. [33], our segmentation mask is both finer in detail and more accurate. Performance on LEVIR [12] is comparable across models, but our method achieves higher precision on the multispectral OSCD dataset [17]. Unlike the optical-only DINOv3 [49], DEO leverages information beyond optical, reducing false positives. Compared to Copernicus-FM [56], it further improves utilization of multispectral information, demonstrating the effectiveness of our dual-teacher paradigm.

Limitations. Our method is to some degree limited by the strength of the optical VFM used for distillation, as optical features are transferred but not explicitly pretrained. It also assumes spatially aligned input, which is valid for op-

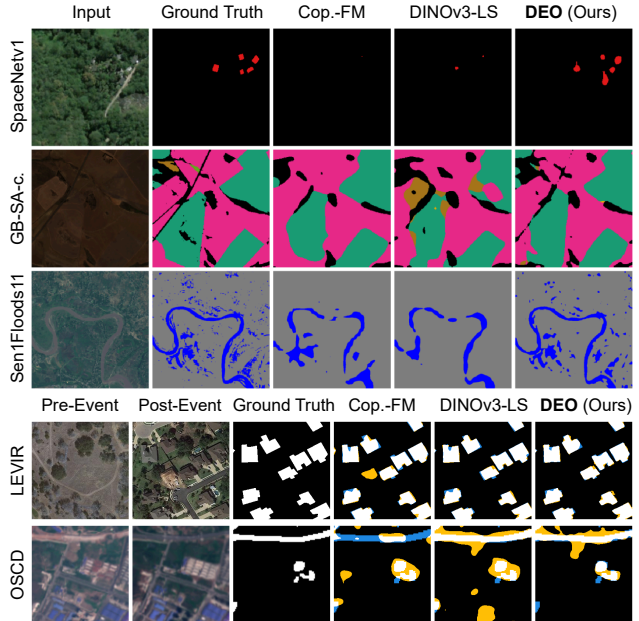


Figure 4. Qualitative results for semantic segmentation. The first two columns contain the optical part of the input image and the ground truth. The final three columns contain predictions from two related models, and our own.

tical and multispectral data, but poses a challenge for sensors from other platforms. Additionally, the lack of a strong teacher for modalities such as SAR limits the method’s extensibility to such modalities. We plan to explore both sensor alignment and temporal alignment through pretraining tasks in the future.

5. Conclusion

We presented a dual-teacher distillation framework for multispectral Earth observation pretraining, DEO, combining a contrastive self-distillation teacher with a vision foundation model (VFM) teacher. This design efficiently transfers high-level semantic knowledge from an optical-only VFM while adapting it to multispectral data through a compatible contrastive learning objective. Unlike prior approaches that couple masked image modeling with VFM distillation, our formulation aligns the student’s training paradigm with that of modern VFMs such as DINOv3, which themselves rely on contrastive self-distillation to produce semantically structured feature spaces. This alignment leads to more coherent cross-modal feature transfer, resulting in improved performance on both optical and multispectral benchmarks, with an average improvement of 3.64 points in semantic segmentation, 1.2 points in change detection, and 1.31 points in classification tasks. These findings highlight distillation-based pretraining as a scalable and resource-efficient path toward an interoperable ecosystem of Earth

observation foundation models.

Acknowledgements

This work was in part supported by the ARIS research projects J2-60045 (RoDEO) and GC-0006 (GeoAI), research programme P2-0214, and the supercomputing network SLING (ARNES, EuroHPC Vega).

References

- [1] Muhammad Sohail anish, Muhammad Akhtar Munir, Syed Roshaan Ali Shah, Muhammad Haris Khan, Rao Muhammad Anwer, Jorma Laaksonen, Fahad Shahbaz Khan, and Salman Khan. Terrafm: A Scalable Foundation Model for Unified Multisensor Earth Observation. In *9th International Conference on Learning Representations, ICLR*, 2026. 1, 2, 5, 6, 8, 14
- [2] Guillaume Astruc, Nicolas Gonthier, Clement Mallet, and Loic Landrieu. Omnisat: Self-Supervised Modality Fusion for Earth Observation. In *European Conference on Computer Vision*, pages 409–427. Springer, 2024. 2
- [3] Guillaume Astruc, Nicolas Gonthier, Clement Mallet, and Loic Landrieu. Anysat: One Earth Observation Model for Many Resolutions, Scales, and Modalities. In *Proceedings of the Computer Vision and Pattern Recognition Conference*, pages 19530–19540, 2025. 1, 2
- [4] Mohammed Baharoon, Waseem Qureshi, Jiahong Ouyang, Yanwu Xu, Abdulrhman Aljouie, and Wei Peng. Evaluating General Purpose Vision Foundation Models for Medical Image Analysis: An Experimental Study of Dinov2 on Radiology Benchmarks. *arXiv preprint arXiv:2312.02366*, 2023. 2
- [5] Randall Balestriero and Yann Lecun. How learning by reconstruction produces uninformative features for perception. In *Proceedings of the 41st International Conference on Machine Learning*, pages 2566–2585. PMLR, 2024. 2, 8
- [6] Adrien Bardes, Jean Ponce, and Yann LeCun. Vircreg: Variance-invariance-covariance regularization for self-supervised learning. In *The Tenth International Conference on Learning Representations, ICLR*, 2022. 2
- [7] Alvard Barseghyan, Ani Vanyan, Hakob Tamazyan, Evan Shelhamer, and Hrant Khachatrian. Less is More? Data Specialization for Self-Supervised Remote Sensing Models. In *TerraBytes-ICML 2025 Workshop*, 2025. 2
- [8] Cristian Bodnar, Wessel P Bruinsma, Ana Lucic, Megan Stanley, Anna Allen, Johannes Brandstetter, Patrick Garvan, Maik Riechert, Jonathan A Weyn, Haiyu Dong, et al. A Foundation Model for the Earth System. *Nature*, pages 1–8, 2025. 1
- [9] Derrick Bonafilia, Beth Tellman, Tyler Anderson, and Erica Issenberg. Sen1floods11: A Georeferenced Dataset to Train and Test Deep Learning Flood Algorithms for Sentinel-1. In *Proceedings of the IEEE/CVF Conference on Computer Vision and Pattern Recognition Workshops*, pages 210–211, 2020. 5, 8, 15
- [10] Christopher F Brown, Michal R Kazmierski, Valerie J Pasquarella, William J Rucklidge, Masha Samsikova, Chenhui Zhang, Evan Shelhamer, Estefania Lahera, Olivia Wiles, Simon Ilyushchenko, et al. Alphaeart Foundations: An Embedding Field Model for Accurate and Efficient Global Mapping From Sparse Label Data. *arXiv preprint arXiv:2507.22291*, 2025. 1
- [11] Mathilde Caron, Hugo Touvron, Ishan Misra, Hervé Jégou, Julien Mairal, Piotr Bojanowski, and Armand Joulin. Emerging Properties in Self-Supervised Vision Transformers. In *Proceedings of the IEEE/CVF International Conference on Computer Vision*, pages 9650–9660, 2021. 2, 3, 4, 5
- [12] Hao Chen and Zhenwei Shi. A Spatial-Temporal Attention-Based Method and A New Dataset for Remote Sensing Image Change Detection. *Remote Sensing*, 12:1662, 2020. 6, 8, 13, 16
- [13] Ting Chen, Simon Kornblith, Mohammad Norouzi, and Geoffrey Hinton. A Simple Framework for Contrastive Learning of Visual Representations. In *International Conference on Machine Learning*, pages 1597–1607. PmLR, 2020. 2, 4
- [14] Xinlei Chen and Kaiming He. Exploring Simple Siamese Representation Learning. In *Proceedings of the IEEE/CVF Conference on Computer Vision and Pattern Recognition*, pages 15750–15758, 2021. 3
- [15] Gordon Christie, Neil Fendley, James Wilson, and Ryan Mukherjee. Functional Map of the World. In *Proceedings of the IEEE Conference on Computer Vision and Pattern Recognition*, pages 6172–6180, 2018. 5
- [16] Yezhen Cong, Samar Khanna, Chenlin Meng, Patrick Liu, Erik Rozi, Yutong He, Marshall Burke, David Lobell, and Stefano Ermon. Satmae: Pre-Training Transformers for Temporal and Multi-Spectral Satellite Imagery. *Advances in Neural Information Processing Systems*, 35:197–211, 2022. 2, 5
- [17] Rodrigo Caye Daudt, Bertr Le Saux, Alexandre Boulch, and Yann Gousseau. Urban Change Detection for Multispectral Earth Observation Using Convolutional Neural Networks. In *IEEE International Geoscience and Remote Sensing Symposium*, pages 2115–2118. IEEE, 2018. 6, 8, 13, 16
- [18] Minh Kha Do, Kang Han, Phu Lai, Khoa T Phan, and Wei Xiang. Robsense: A Robust Multi-Modal Foundation Model for Remote Sensing With Static, Temporal, and Incomplete Data Adaptability. In *Proceedings of the Computer Vision and Pattern Recognition Conference*, pages 7427–7436, 2025. 1, 2
- [19] Alexey Dosovitskiy, Lucas Beyer, Alexander Kolesnikov, Dirk Weissenborn, Xiaohua Zhai, Thomas Unterthiner, Mostafa Dehghani, Matthias Minderer, Georg Heigold, Sylvain Gelly, Jakob Uszkoreit, and Neil Houlsby. An image is worth 16x16 words: Transformers for image recognition at scale. In *9th International Conference on Learning Representations, ICLR*, 2021. 5
- [20] Ibrahim Fayad, Max Zimmer, Martin Schwartz, Fabian Gieseke, Philippe Ciais, Gabriel Belouze, Sarah Brood, Aurélien de Truchis, and Alexandre d’Aspremont. DUNIA: pixel-sized embeddings via cross-modal alignment for earth observation applications. In *Forty-second International Conference on Machine Learning, ICML*, 2025. 1, 2
- [21] Anthony Fuller, Koreen Millard, and James Green. Croma: Remote Sensing Representations With Contrastive Radar-

- Optical Masked Autoencoders. *Advances in Neural Information Processing Systems*, 36:5506–5538, 2023. 2, 5, 6, 8, 14
- [22] Vivien Sainte Fare Garnot and Loic Landrieu. Panoptic Segmentation of Satellite Image Time Series With Convolutional Temporal Attention Networks. In *Proceedings of the IEEE/CVF International Conference on Computer Vision*, pages 4872–4881, 2021. 5, 15
- [23] Ziyang Gong, Zhixiang Wei, Di Wang, Xiaoxing Hu, Xianzheng Ma, Hongruixuan Chen, Yuru Jia, Yupeng Deng, Zhenming Ji, Xiangwei Zhu, et al. Crossearth: Geospatial vision foundation model for domain generalizable remote sensing semantic segmentation. *IEEE Transactions on Pattern Analysis and Machine Intelligence*, 2025. 2
- [24] Jean-Bastien Grill, Florian Strub, Florent Altché, Corentin Tallec, Pierre Richemond, Elena Buchatskaya, Carl Doersch, Bernardo Avila Pires, Zhaohan Guo, Mohammad Gheshlaghi Azar, et al. Bootstrap Your Own Latent—a New Approach to Self-Supervised Learning. *Advances in neural information processing systems*, 33:21271–21284, 2020. 2, 3
- [25] Boran Han, Shuai Zhang, Xingjian Shi, and Markus Reichstein. Bridging Remote Sensors With Multisensor Geospatial Foundation Models. In *Proceedings of the IEEE/cvf Conference on Computer Vision and Pattern Recognition*, pages 27852–27862, 2024. 2
- [26] Kaiming He, Haoqi Fan, Yuxin Wu, Saining Xie, and Ross Girshick. Momentum Contrast for Unsupervised Visual Representation Learning. In *Proceedings of the IEEE/CVF Conference on Computer Vision and Pattern Recognition*, pages 9729–9738, 2020. 2, 3
- [27] Kaiming He, Xinlei Chen, Saining Xie, Yanghao Li, Piotr Dollár, and Ross Girshick. Masked Autoencoders Are Scalable Vision Learners. In *Proceedings of the IEEE/CVF Conference on Computer Vision and Pattern Recognition*, pages 16000–16009, 2022. 2
- [28] Greg Heinrich, Mike Ranzinger, Hongxu Yin, Yao Lu, Jan Kautz, Andrew Tao, Bryan Catanzaro, and Pavlo Molchanov. Radio2. 5: Improved Baselines for Agglomerative Vision Foundation Models. In *Proceedings of the Computer Vision and Pattern Recognition Conference*, pages 22487–22497, 2025. 2, 7
- [29] Yuru Jia, Valerio Marsocci, Ziyang Gong, Xue Yang, Maarten Vergauwen, and Andrea Nascetti. Can generative geospatial diffusion models excel as discriminative geospatial foundation models? In *Proceedings of the IEEE/CVF International Conference on Computer Vision*, pages 8429–8440, 2025. 1, 2, 5, 6, 8, 14
- [30] Samar Khanna, Patrick Liu, Linqi Zhou, Chenlin Meng, Robin Rombach, Marshall Burke, David B. Lobell, and Stefano Ermon. Diffusionsat: A generative foundation model for satellite imagery. In *The Twelfth International Conference on Learning Representations*, 2024. 2
- [31] Diederik P. Kingma and Jimmy Ba. Adam: A method for stochastic optimization. In *3rd International Conference on Learning Representations, ICLR*, 2015. 5
- [32] Alexander Kirillov, Eric Mintun, Nikhila Ravi, Hanzi Mao, Chloe Rolland, Laura Gustafson, Tete Xiao, Spencer Whitehead, Alexander C Berg, Wan-Yen Lo, et al. Segment Anything. In *Proceedings of the IEEE/CVF International Conference on Computer Vision*, pages 4015–4026, 2023. 2
- [33] Alexandre Lacoste, Nils Lehmann, Pau Rodriguez, Evan Sherwin, Hannah Kerner, Björn Lütjens, Jeremy Irvin, David Dao, Hamed Alemohammad, Alexandre Drouin, et al. Geobench: Toward Foundation Models for Earth Monitoring. *Advances in Neural Information Processing Systems*, 36: 51080–51093, 2023. 1, 5, 6, 8, 13, 15, 16
- [34] Yansheng Li, Xinwei Li, Yongjun Zhang, Daifeng Peng, and Lorenzo Bruzzone. Cost-efficient Information Extraction From Massive Remote Sensing Data: When Weakly Supervised Deep Learning Meets Remote Sensing Big Data. *International Journal of Applied Earth Observation and Geoinformation*, 120:103345, 2023. 1
- [35] Zhihao Li, Biao Hou, Siteng Ma, Zitong Wu, Xianpeng Guo, Bo Ren, and Licheng Jiao. Masked Angle-Aware Autoencoder for Remote Sensing Images. In *European Conference on Computer Vision*, pages 260–278. Springer, 2024. 2
- [36] Ze Liu, Yutong Lin, Yue Cao, Han Hu, Yixuan Wei, Zheng Zhang, Stephen Lin, and Baining Guo. Swin Transformer: Hierarchical Vision Transformer Using Shifted Windows. In *Proceedings of the IEEE/CVF International Conference on Computer Vision*, pages 10012–10022, 2021. 5
- [37] Matías Mendieta, Boran Han, Xingjian Shi, Yi Zhu, and Chen Chen. Towards Geospatial Foundation Models via Continual Pretraining. In *Proceedings of the IEEE/CVF International Conference on Computer Vision*, pages 16806–16816, 2023. 2, 4, 5, 6, 8, 14
- [38] SF Meneses III and AC Blanco. Rapid Mapping and Assessment of Damages Due to Typhoon Rai Using Sentinel-1 Synthetic Aperture Radar Data. *The International Archives of the Photogrammetry, Remote Sensing and Spatial Information Sciences*, 43:1139–1146, 2022. 8
- [39] Aaron van den Oord, Yazhe Li, and Oriol Vinyals. Representation Learning With Contrastive Predictive Coding. *arXiv preprint arXiv:1807.03748*, 2018. 2
- [40] Maxime Oquab, Timothée Darcet, Théo Moutakanni, Huy V. Vo, Marc Szafraniec, Vasil Khalidov, Pierre Fernandez, Daniel HAZIZA, Francisco Massa, Alaaeldin El-Nouby, Mido Assran, Nicolas Ballas, Wojciech Galuba, Russell Howes, Po-Yao Huang, Shang-Wen Li, Ishan Misra, Michael Rabbat, Vasu Sharma, Gabriel Synnaeve, Hu Xu, Herve Jegou, Julien Mairal, Patrick Labatut, Armand Joulin, and Piotr Bojanowski. DINOv2: Learning robust visual features without supervision. *Transactions on Machine Learning Research*, 2024. Featured Certification. 2, 3, 5, 6, 7, 8, 14
- [41] Alec Radford, Jong Wook Kim, Chris Hallacy, Aditya Ramesh, Gabriel Goh, Sandhini Agarwal, Girish Sastry, Amanda Askell, Pamela Mishkin, Jack Clark, et al. Learning Transferable Visual Models From Natural Language Supervision. In *International Conference on Machine Learning*, pages 8748–8763. PmLR, 2021. 2
- [42] Mike Ranzinger, Greg Heinrich, Jan Kautz, and Pavlo Molchanov. Am-radio: Agglomerative Vision Foundation Model Reduce All Domains Into One. In *Proceedings of the IEEE/CVF Conference on Computer Vision and Pattern Recognition*, pages 12490–12500, 2024. 2

- [43] Colorado J Reed, Ritwik Gupta, Shufan Li, Sarah Brockman, Christopher Funk, Brian Clipp, Kurt Keutzer, Salvatore Candido, Matt Uyttendaele, and Trevor Darrell. Scale-mae: A Scale-Aware Masked Autoencoder for Multiscale Geospatial Representation Learning. In *Proceedings of the IEEE/CVF International Conference on Computer Vision*, pages 4088–4099, 2023. 1, 2, 5, 6, 8, 14
- [44] Esther Rolf, Konstantin Klemmer, Caleb Robinson, and Hannah Kerner. Position: Mission Critical–Satellite Data is a Distinct Modality in Machine Learning. In *Forty-first International Conference on Machine Learning*, 2024. 1
- [45] Blaž Rolih, Matic Fučka, Filip Wolf, and Luka Čehovin Zajc. Be the Change You Want to See: Revisiting Remote Sensing Change Detection Practices. *IEEE Transactions on Geoscience and Remote Sensing*, 63:1–11, 2025. 6, 14
- [46] Olaf Ronneberger, Philipp Fischer, and Thomas Brox. U-net: Convolutional networks for biomedical image segmentation. In *International Conference on Medical image computing and computer-assisted intervention*, pages 234–241. Springer, 2015. 14
- [47] Mert Bülent Saryıldız, Philippe Weinzaepfel, Thomas Lucas, Pau de Jorje, Diane Larlus, and Yannis Kalantidis. Dune: Distilling a Universal Encoder From Heterogeneous 2d and 3d Teachers. In *Proceedings of the Computer Vision and Pattern Recognition Conference*, pages 30084–30094, 2025. 2
- [48] Shashank Shekhar, Florian Bordes, Pascal Vincent, and A Morcos. Understanding Contrastive Versus Reconstructive Self-Supervised Learning of Vision Transformers. In *NeurIPS 2022 Workshop: Self-Supervised Learning—Theory and Practice 2022*, 2022. 8
- [49] Oriane Siméoni, Huy V Vo, Maximilian Seitzer, Federico Baldassarre, Maxime Oquab, Cijo Jose, Vasil Khalidov, Marc Szafraniec, Seungeun Yi, Michaël Ramamonjisoa, et al. Dinov3. *arXiv preprint arXiv:2508.10104*, 2025. 2, 3, 4, 5, 6, 7, 8, 14
- [50] Gabriel Tseng, Anthony Fuller, Marlena Reil, Henry Herzog, Patrick Beukema, Favyen Bastani, James R Green, Evan Shelhamer, Hannah Kerner, and David Rolnick. Galileo: Learning global & local features of many remote sensing modalities. In *Forty-second International Conference on Machine Learning*, 2025. 1, 2, 5
- [51] Dimitris Valsamis, Alexandros Oikonomidis, Chrysoula Chatzichristaki, Anastasia Moutzidou, Ilias Gialampoukidis, Stefanos Vrochidis, and Ioannis Kompatsiaris. Towards Advanced Wildfire Analysis: A Siamese Network-Based Change Detection Approach Through Self-Supervised Learning. In *2024 International Conference on Content-Based Multimedia Indexing (CBMI)*, pages 1–7. IEEE, 2024. 8
- [52] Adam Van Etten, Dave Lindenbaum, and Todd M Bacastow. Spacenet: A Remote Sensing Dataset and Challenge Series. *arXiv preprint arXiv:1807.01232*, 2018. 1, 5, 8, 15
- [53] Leonard Waldmann, Ando Shah, Yi Wang, Nils Lehmann, Adam Stewart, Zhitong Xiong, Xiao Xiang Zhu, Stefan Bauer, and John Chuang. Panopticon: Advancing Any-Sensor Foundation Models for Earth Observation. In *Proceedings of the Computer Vision and Pattern Recognition Conference*, pages 2204–2214, 2025. 1, 2, 4
- [54] Di Wang, Jing Zhang, Minqiang Xu, Lin Liu, Dongsheng Wang, Erzhong Gao, Chengxi Han, Haonan Guo, Bo Du, Dacheng Tao, et al. MTP: Advancing Remote Sensing Foundation Model via Multi-Task Pretraining. *IEEE Journal of Selected Topics in Applied Earth Observations and Remote Sensing*, 2024. 6, 14
- [55] Yi Wang, Conrad M Albrecht, and Xiao Xiang Zhu. Multi-label Guided Soft Contrastive Learning for Efficient Earth Observation Pretraining. *IEEE Transactions on Geoscience and Remote Sensing*, 2024. 2
- [56] Yi Wang, Zhitong Xiong, Chenying Liu, Adam J Stewart, Thomas Dujardin, Nikolaos Ioannis Bountos, Angelos Zavras, Franziska Gerken, Ioannis Papoutsis, Laura Leal-Taixé, et al. Towards a Unified Copernicus Foundation Model for Earth Vision. In *Proceedings of the IEEE/CVF International Conference on Computer Vision*, 2025. 1, 2, 4, 5, 6, 8, 14
- [57] Xinye Wanyan, Sachith Seneviratne, Shuchang Shen, and Michael Kirley. Extending Global-Local View Alignment for Self-Supervised Learning With Remote Sensing Imagery. In *Proceedings of the IEEE/CVF Conference on Computer Vision and Pattern Recognition*, pages 2443–2453, 2024. 2
- [58] Ziyang Wu, Jingyuan Zhang, Druv Pai, XuDong Wang, Chandan Singh, Jianwei Yang, Jianfeng Gao, and Yi Ma. Simplifying DINO via Coding Rate Regularization. In *Forty-second International Conference on Machine Learning*, 2025. 2, 3, 13
- [59] Aoran Xiao, Weihao Xuan, Junjue Wang, Jiaying Huang, Dacheng Tao, Shijian Lu, and Naoto Yokoya. Foundation Models for Remote Sensing and Earth Observation: A Survey. *IEEE Geoscience and Remote Sensing Magazine*, 2025. 1
- [60] Tete Xiao, Yingcheng Liu, Bolei Zhou, Yuning Jiang, and Jian Sun. Unified Perceptual Parsing for Scene Understanding. In *Proceedings of the European Conference on Computer Vision (ECCV)*, pages 418–434, 2018. 5, 6, 14
- [61] Zhenda Xie, Zheng Zhang, Yue Cao, Yutong Lin, Jianmin Bao, Zhuliang Yao, Qi Dai, and Han Hu. Simmim: A Simple Framework for Masked Image Modeling. In *Proceedings of the IEEE/CVF Conference on Computer Vision and Pattern Recognition*, pages 9653–9663, 2022. 2
- [62] Zhitong Xiong, Yi Wang, Fahong Zhang, Adam J Stewart, Joëlle Hanna, Damian Borth, Ioannis Papoutsis, Bertrand Le Saux, Gustau Camps-Valls, and Xiao Xiang Zhu. Neural Plasticity-Inspired Foundation Model for Observing the Earth Crossing Modalities. *CoRR*, 2024. 2
- [63] Zhitong Xiong, Yi Wang, Fahong Zhang, and Xiao Xiang Zhu. One for All: Toward Unified Foundation Models for Earth Vision. In *IGARSS 2024-2024 IEEE International Geoscience and Remote Sensing Symposium*, pages 2734–2738. IEEE, 2024. 1
- [64] Jure Zbontar, Li Jing, Ishan Misra, Yann LeCun, and Stéphane Deny. Barlow Twins: Self-Supervised Learning via Redundancy Reduction. In *International Conference on Machine Learning*, pages 12310–12320. PMLR, 2021. 2, 4
- [65] Yingying Zhang, Lixiang Ru, Kang Wu, Lei Yu, Lei Liang, Yansheng Li, and Jingdong Chen. SkySense V2: A Uni-

fied Foundation Model for Multi-Modal Remote Sensing. In *Proceedings of the IEEE/CVF International Conference on Computer Vision*, 2025. [1](#), [2](#)

- [66] Jinghao Zhou, Chen Wei, Huiyu Wang, Wei Shen, Cihang Xie, Alan Yuille, and Tao Kong. ibot: Image bert pre-training with online tokenizer. *International Conference on Learning Representations (ICLR)*, 2022. [2](#)

Brewing Stronger Features: Dual-Teacher Distillation for Multispectral Earth Observation

Supplementary Material

A. Pretraining

In this section, we will expand on the pretraining methodology and details introduced in Section 3. We will first provide more insight into our pretraining methodology, followed by details on hyperparameters to aid in reproducibility.

A.1. Contrastive self-distillation

The full loss for the *coding rate regularizer* [58] described in Section 3.1 can be formulated as:

$$\mathcal{L}_{\text{CR}} = -\frac{p + NB}{pNB} \frac{1}{V} \sum_{i=1}^V \log \det \left(\mathbf{I}_p + \frac{p}{BN\varepsilon} z_i^\top z_i \right), \quad (6)$$

where $z_i^\top z_i$ represents the covariance matrix, and $\log \det$ is calculated using the Cholesky expansion, i.e.,

$$\log \det(A) = 2 \sum_{i=1}^p \log L_{ii}. \quad (7)$$

Here, L_{ii} are diagonal elements of the matrix L that satisfies the Cholesky decomposition $A = LL^\top$. B represents the batch size, while N is the number of used GPUs. p is the dimension of the features z after projection (256 for MS learning). Since \mathcal{L}_{CR} is calculated only on the global student and teacher views, $V = 2$. Finally, ε is a small constant used for balancing, here 0.05. The first factor $\frac{p+NB}{pNB}$ is a heuristic to balance the loss and can be adjusted accordingly.

Parameter	Value
n	2
m	10
α_1	1
α_2	0.5
α_3	0.5
γ	1
EMA	0.996
Cos scheduler WD	0.04
Base LR	0.0005
Warmup epochs	10

Table 8. Details of pretraining hyperparameters.

Element	Value
Swin	
Input patch size	4
Embedding dim.	128
Windows size	12
Projection head	
Hidden dim.	2048
Bottleneck dim. (MS)	256
Bottleneck dim. (Optical)	1024

Table 9. Network element sizes.

A.2. Hyperparameters

In Table 8 we provide details about the hyperparameters used during pretraining. In Table 9 we provide details about the sizes of network elements.

B. Evaluation

In this section, we provide additional details about the datasets used for evaluation, as well as a more detailed description of our evaluation methodology.

B.1. Datasets

Semantic segmentation. For semantic segmentation, we use a mixture of established benchmarks in the form of GEO-Bench [33] and standalone datasets. Details are provided in Table 12.

Classification. We use three multispectral classification datasets from the GEO-Bench [33] benchmark. m-bigearthnet is a multi-label classification task, while m-so2sat and m-eurosat are single-label classification tasks. We provide details in Table 13.

Change detection. We use the optical LEVIR [12] and multispectral OCSD [17] change detection datasets. Details are provided in Table 14.

Parameter	Value
Pool scales	1, 2, 3, 6
Hidden size	512

Table 10. Details of the UPerNet segmentation head.

B.2. Evaluation details

For all experiments, we use a batch size of 64 and fine-tune for 50 epochs using a learning rate. We provide other details in the following section.

Semantic segmentation. For all methods, we fine-tune an UPerNet [60] segmentation head on top of a frozen backbone. We extract features from four stages of the backbone: for ViT-B backbones, these are stages 3, 5, 8, and 11; for ViT-L, stages 7, 11, 15, and 23; and for Swin-based backbones, we take the four Swin stages before pooling. For ViT backbones, the latest stage is downsampled, while the first and second stages are upsampled four times and 2 times, respectively. UPerNet details are provided in Table 10.

Classification. We extract the last layer features from a frozen backbone and train a simple linear layer on top of them. For ViT backbones, we extract the last layer class token, while for Swin backbones, we pool the last layer features to simulate a class token.

Change detection. For all evaluated methods, we first perform backbone feature fusion of a pair of images using a simple element-wise subtraction. We then pass them to a UPerNet [60], except for ViT-based methods, where we use the UNet [46] decoder, as it performs better. Following related work [45, 54], we also train the backbone for change detection. We extract features from four stages for all models: for ViT-B backbones, these are stages 3, 5, 7, and 11; for ViT-L, stages 7, 11, 15, and 23; and for Swin-based backbones, we take the four Swin stages before pooling. UPerNet details are provided in Table 10 and for UNet we use the same setup as in [45].

Dataset	LR	
	Other methods	SatDiFuser
m-pv4ger-seg	10^{-4}	10^{-2}
m-chesapeake-landcover	10^{-4}	10^{-2}
m-cashew-plantation	10^{-2}	10^{-2}
m-SA-crop-type	10^{-4}	10^{-2}
m-nz-cattle	10^{-4}	10^{-3}
SpaceNetv1	10^{-4}	10^{-2}
Sen1Floods11	10^{-4}	10^{-2}
PASTIS	10^{-1}	10^{-2}
m-bigearthnet	10^{-3}	10^{-2}
m-so2sat	10^{-3}	10^{-4}
m-eurosat	10^{-2}	10^{-2}
LEVIR-CD	10^{-4}	10^{-4}
OSCD	10^{-4}	10^{-4}

Table 11. Learning rates for datasets and methods.

C. Method details

We implement each evaluated method using its official repository. We use consistent learning rates per method, except for SatDiFuser [29], for which we use the provided learning rates. Learning rates are presented in Table 11. Official repositories of evaluated methods are listed in the following:

- DINOv2 [40]: <https://github.com/facebookresearch/dinov2>
- DINOv3 [49]: <https://github.com/facebookresearch/dinov3>
- Scale-MAE [43]: <https://github.com/bair-climate-initiative/scale-mae>
- GFM [37]: <https://github.com/mmendiet/GFM>
- SatDiFuser [29]: <https://github.com/yurujaja/SatDiFuser>
- CROMA [21]: <https://github.com/antofuller/CROMA/tree/main>
- TerraFM [1]: <https://github.com/mbzuai-oryx/TerraFM/blob/master/terrafm.py>
- Copernicus-FM [56]: <https://github.com/zhu-xlab/Copernicus-FM>

D. Additional qualitative

We provide additional qualitative results in Figures 5 to 8.

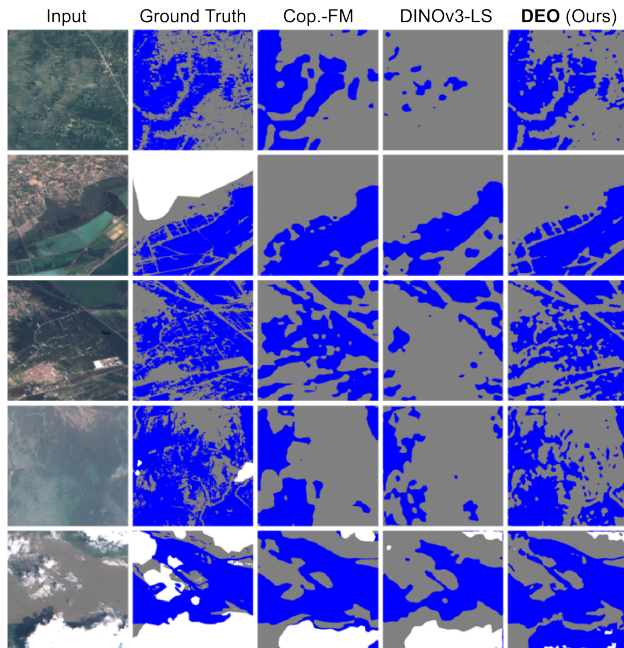


Figure 5. Extended qualitative results for Sen1Floods11.

Segmentation

GEO-Bench [33]	In paper	Image Size	# Classes	Train	Val	Test	# Bands	RGB res	Sensors
m-pv4ger-seg	GB-pv	320×320	2	3000	403	403	3	0.1	RGB
m-chesapeake-landcover	GB-chesa.	256×256	7	3000	1000	1000	4	1.0	RGBN
m-cashew-plantation	GB-cas.	256×256	7	1350	400	50	13	10.0	Sentinel-2
m-SA-crop-type	GB-SA-c.	256×256	10	3000	1000	1000	13	10.0	Sentinel-2
m-nz-cattle	GB-cattle	500×500	2	524	66	65	3	0.1	RGB
Others									
SpaceNetv1 [52]	SN	224×224	2	5000	1000	1000	3	0.5	DigitalGlobe WorldView 2
Sen1Floods11 [9]	S1F11	512×512	3	252	89	90	13	10.0	Sentinel-2
PASTIS [22]	PASTIS	128×128	20	1455	482	496	10	10.0	Sentinel-2

Table 12. Details for segmentation datasets used in the paper for evaluation.

Classification

GEO-Bench [33]	In paper	Image Size	# Classes	Train	Val	Test	# Bands	RGB res	Sensors
m-bigearthnet	GB-ben	120×120	43	20000	1000	1000	12	10.0	Sentinel-2
m-so2sat	GB-s2s	32×32	17	19992	986	986	18	1.0	Sen.-2 + Sen.-1
m-eurosat	GB-es	64×64	10	2000	1000	1000	13	10.0	Sentinel-2

Table 13. Details for classification datasets used in the paper for evaluation.

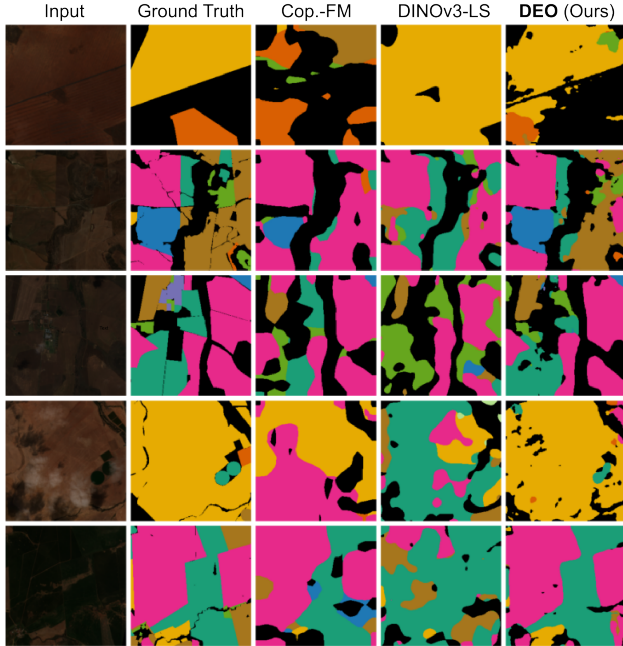


Figure 6. Extended qualitative results for m-SA-crop-type.

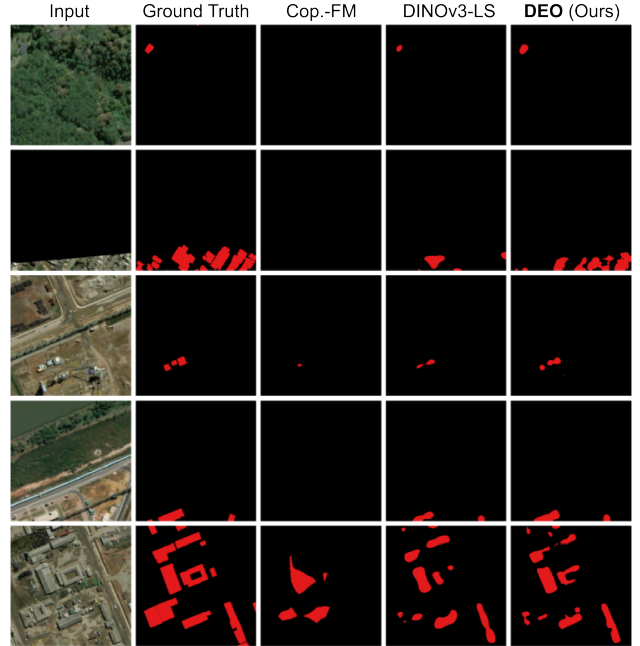


Figure 7. Extended qualitative results for SpaceNetv1.

Change detection

GEO-Bench [33]	In paper	Image Size	# Classes	Train	Val	Test	# Bands	RGB res	Sensors
LEVIR-CD [12]	LEVIR	256×256	2	7120	1024	2048	3	0.5	Google Earth satellite
OSCD [17]	OSCD	96×96	2	827	-	385	10	10.0	Sentinel 2

Table 14. Details for change detection datasets used in the paper for evaluation.

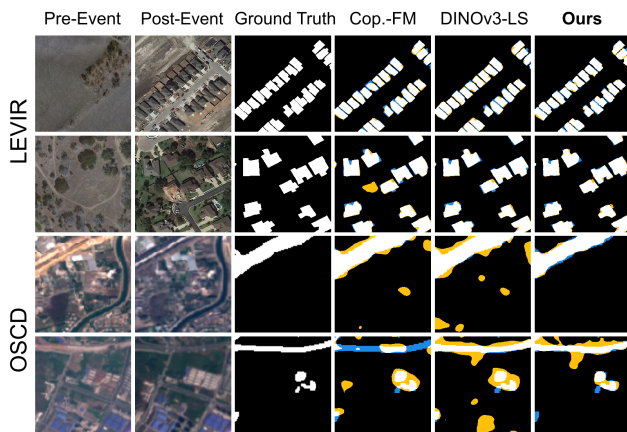


Figure 8. Extended qualitative results for LEVIR and OSCD.